

This is the accepted manuscript made available via CHORUS. The article has been published as:

## “Ultracold” Neutral Plasmas at Room Temperature

N. Heilmann, J. B. Peatross, and S. D. Bergeson

Phys. Rev. Lett. **109**, 035002 — Published 16 July 2012

DOI: [10.1103/PhysRevLett.109.035002](https://doi.org/10.1103/PhysRevLett.109.035002)

# “Ultracold” neutral plasmas at room temperature

N. Heilmann, J. B. Peatross, and S. D. Bergeson\*

*Department of Physics and Astronomy, Brigham Young University, Provo, UT 84602, USA*

(Dated: May 4, 2012)

We report a measurement of the electron temperature in a plasma generated by a high-intensity laser focused into a jet of neon. The 15 eV electron temperature is determined using an analytic solution of the plasma equations assuming local thermodynamic equilibrium, initially developed for ultracold neutral plasmas. We show that this analysis method accurately reproduces more sophisticated plasma simulations in our temperature and density range. While our plasma temperatures are far outside the typical “ultracold” regime, the ion temperature is determined by the plasma density through disorder-induced heating just as in ultracold neutral plasma experiments. Based on our results we outline a pathway for achieving a strongly coupled neutral laser-produced plasma that even more closely resembles ultracold neutral plasma conditions.

PACS numbers: 52.27.Gr, 52.20.-j, 79.70.+q, 52.25.Jm

Laser-produced plasmas (LPPs) span a wide range of temperatures and densities [1]. At one extreme, lasers are used to achieve fusion conditions [2] with plasma densities near  $n = 10^{23} \text{ cm}^{-3}$ . Today's highest intensity lasers can be used to generate electrons with kinetic energies up to  $k_B T_e = 400 \text{ MeV}$  using laser wakefield acceleration [3]. On the other extreme of temperature and density, recent ultracold neutral plasma (UNP) experiments [4–10] generate plasmas with densities near  $n \sim 10^9 \text{ cm}^{-3}$  and electron temperatures as low as  $T_e = 1 \text{ K}$ .

Determining the electron temperature  $T_e$  in LPPs can be difficult [11]. For modest laser intensities  $I = 10^{14} - 10^{16} \text{ W/cm}^2$  and relatively low densities  $n = 10^{15} - 10^{20} \text{ cm}^{-3}$ , ionization of the neutral atoms occurs primarily in the strong-field (multi-photon ionization) regime [12]. When these cool ( $k_B T_e \sim 10 \text{ eV}$ ) low-density plasmas are generated using femtosecond duration laser pulses, they are in a non-equilibrium state. Thermalization, expansion, recombination, and other processes occur on time scales that are long compared to the laser pulse. The electron temperature is often determined by simulating the plasma evolution using the electron and ion fluid equations [13] and comparing with the measured time-dependent density.

Determining the electron temperature is comparatively simple in UNPs [14]. The UNPs are generated by resonantly ionizing laser-cooled gases or gases in supersonic expansions near threshold [4–6, 8, 9]. The  $\sim 1 \text{ mK}$  atomic temperature before ionization make it possible to use narrowband laser excitation to promote the bound electron to low energy continuum states with high efficiency. As long as electron-ion recombination and electron-Rydberg atom scattering can be neglected [14], the electron energy is equal to the difference between the energy of the single photon used to ionize the atoms and the atomic ionization potential. Similarly to the cool low density LPPs, these plasmas are formed in a non-equilibrium state and the relaxation processes occur on time scales that are long compared to the plasma formation time. In this letter we will show that the analysis originally developed for UNPs can be accurately applied to a certain class of low-density, low-temperature LPPs to determine the electron temperature. Strongly-coupled neutral plasmas can be created in these LPPs under the right conditions.

If the electron temperature is not known apriori, the rate at which the plasma expands can be used to determine the electron temperature [14–18]. For UNPs, the expansion rate is derived analytically. The time-dependent spatial density profile in these spherically symmetric plasmas is

$$n(r, t) = n_0 \left( \frac{\sigma_0}{\sigma(t)} \right)^3 \exp \left[ -\frac{r^2}{2\sigma^2(t)} \right], \quad (1)$$

where  $\sigma(t) = (\sigma_0^2 + v_{\text{exp}}^2 t^2)^{1/2}$  and the expansion velocity is  $v_{\text{exp}} = \sqrt{k_B T_e / m_i}$ . Measuring the time-dependent density and fitting it to the form

$$n(t) = \frac{n(0)}{[1 + (v_{\text{exp}} t / \sigma_0)^2]^{3/2}}, \quad (2)$$

gives the electron temperature [14].

This simple UNP expansion theory can be applied to cool low-density LPPs as well, provided a few conditions can be met. First, the UNP theory is valid when the electron temperature is well-defined, meaning that the electrons have a Maxwellian velocity distribution and have a Boltzmann spatial distribution,  $n_e \propto \exp[e\Phi / k_B T_e]$ . Second, the ions are also assumed to have a Maxwellian velocity distribution and to be well-described by fluid equations. This requires the number of particles per Debye sphere to be large ( $n\lambda_D^3 \gg 1$ , where the Debye length is  $\lambda_D = \sqrt{k_B T_e \epsilon_0 / ne^2}$ ), and for collisions between particles to be rapid compared to the plasma expansion. For a cool low-density LPP with  $n = 10^{18} \text{ cm}^{-3}$  and  $k_B T_e = 10 \text{ eV}$ , we find  $n\lambda_D^3 = 13$ . The electron collision rates are  $10^{11} - 10^{12} \text{ s}^{-1}$ . The ion collision rate is  $10^9 \text{ s}^{-1}$  and the ion plasma frequency is  $3 \times 10^{11} \text{ s}^{-1}$ . These rates are high compared the expansion time of a few ns [18].

Third, the electron-ion recombination and electron-Rydberg atom scattering is assumed to be negligible [19]. For a cool low-density LPP with  $n = 10^{18} \text{ cm}^{-3}$  and  $k_B T_e = 10 \text{ eV}$ , the radiative recombination rate is  $9 \times 10^5 \text{ s}^{-1}$  and the three-body recombination rate is  $3 \times 10^5 \text{ s}^{-1}$  [20]. Both are completely negligible on the ns time scale.

The final condition for the validity of the UNP expansion model is that the spatial density distribution should be Gaussian, as in Eq. (1). This condition is not strictly met for LPPs, where cylindrical symmetry is used. In the transverse (radial) direction, the initial spatial distribution is more flat-topped than Gaussian [18], although the deviations from Gaussian do not appear to be large. With appropriate changes for dimensionality, and with the caveat that the density in Eq. (2) refers to the rms density of the plasma, we will show that the UNP expansion model matches the density data and provides a reasonable estimate of the electron temperature.

As an example, we apply Eq. (2) to data published recently by Kanter, et al. [18], that studied the expansion of a cool low-density LPP. In that experiment, a ti:sapphire ultrashort laser pulse propagating in the  $z$  direction was

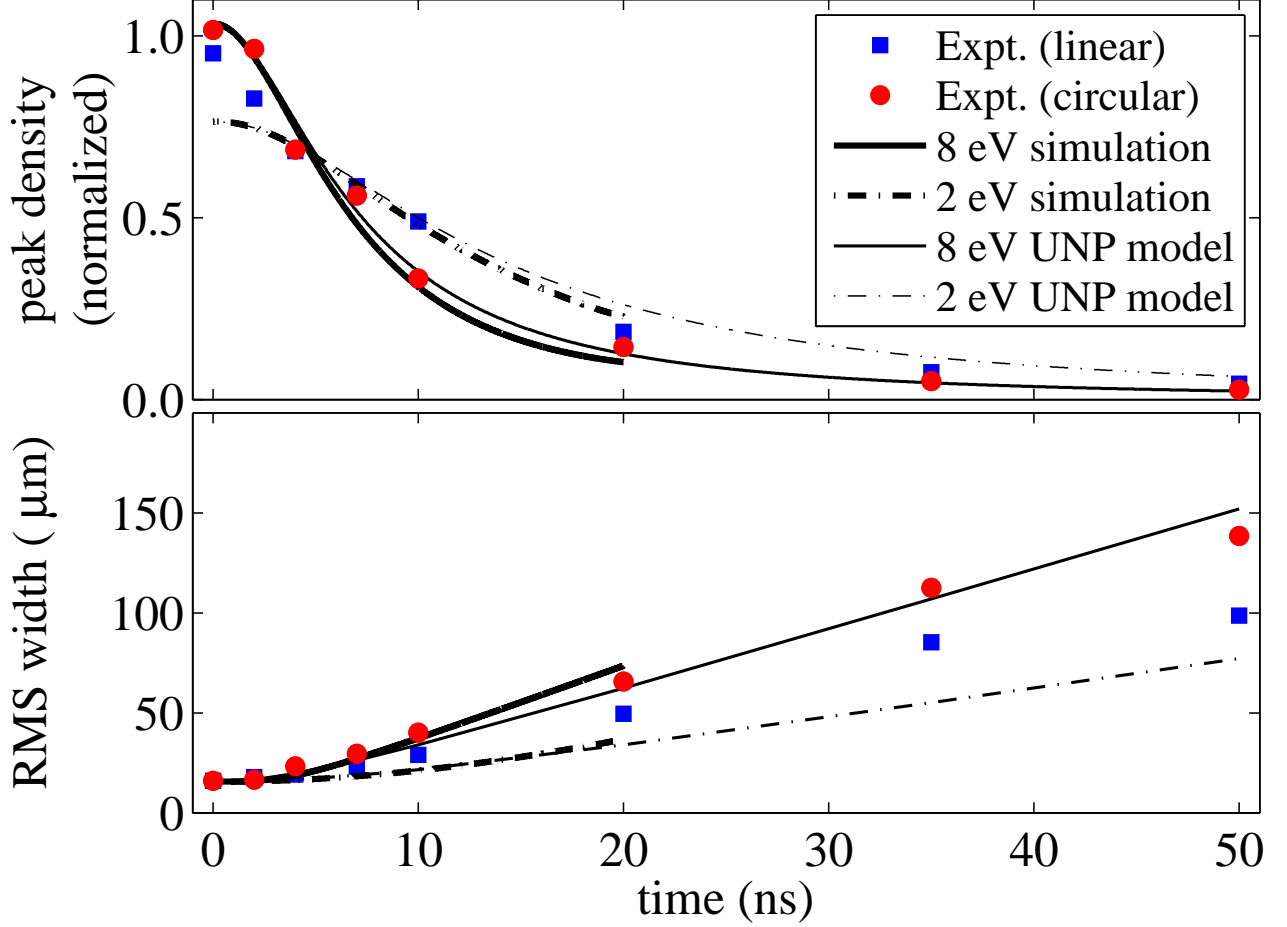


FIG. 1. (color) A comparison of the data and models Ref. [18] with the UNP expansion model. The blue squares and red circles are measured data when the fs laser is linearly and circularly polarized, respectively. The dark lines running from 1 to 20 ns are the simulation from Ref. [18]. The thin lines running from 1 to 50 ns are the UNP model predictions from Eq. (3).

focused asymmetrically to a FWHM in the  $xy$  plane of  $92 \times 46 \mu\text{m}^2$ . Their target was a Kr jet at a density of  $10^{14} \text{ cm}^{-3}$ . At early times the expansion occurs primarily in the  $xy$  plane. Assuming that the plasma has the same relative size as the laser focus, Eq. (2) should be modified for Kanter's experimental parameters to be [21, 22]

$$n_K(t) \approx \frac{n_0}{\sqrt{1 + (v_{\text{exp}} t / \sigma_x)^2} \sqrt{1 + (v_{\text{exp}} t / \sigma_y)^2}} \quad (3)$$

where  $\sigma_x = 16 \mu\text{m}$  and  $\sigma_y = 32 \mu\text{m}$  are the initial rms sizes of the plasma in the  $x$ - and  $y$ -directions [23].

A plot of Kanter's plasma density as a function of time is shown in Fig. 1 for two different laser polarizations. Also plotted is Kanter's simulation (thick black lines from 0 to 20 ns) along with the UNP expansion model of Eq. (3) (thin black lines from 0 to 50 ns). The good agreement between these models indicates that the UNP expansion model can be used to extract meaningful electron temperatures in LPPs.

Applying the UNP expansion model to cool low-density LPPs requires a measurement of the time-evolving plasma density. The beautiful x-ray technique in Ref. [18] is typically not available in most laser laboratories, and interferometry is often used instead. In our lab we also use interferometry to measure the plasma density, as described below.

We generate our plasmas by focusing 4 mJ, 35 fs-duration, ti:sapphire laser pulse effusive pulsed Ne jet. The atom density in the jet ranges up to  $n = 1.5 \times 10^{18} \text{ cm}^{-3}$ . The jet is formed using a solenoid valve with a  $30 \mu\text{m}$  diameter and 2 mm length tube serving as the nozzle. The pressure behind the solenoid ranges up to 1000 Torr. The Ne atoms are ionized when the laser intensity is greater than  $8.7 \times 10^{14} \text{ W/cm}^2$ . We avoid generating higher charge states by

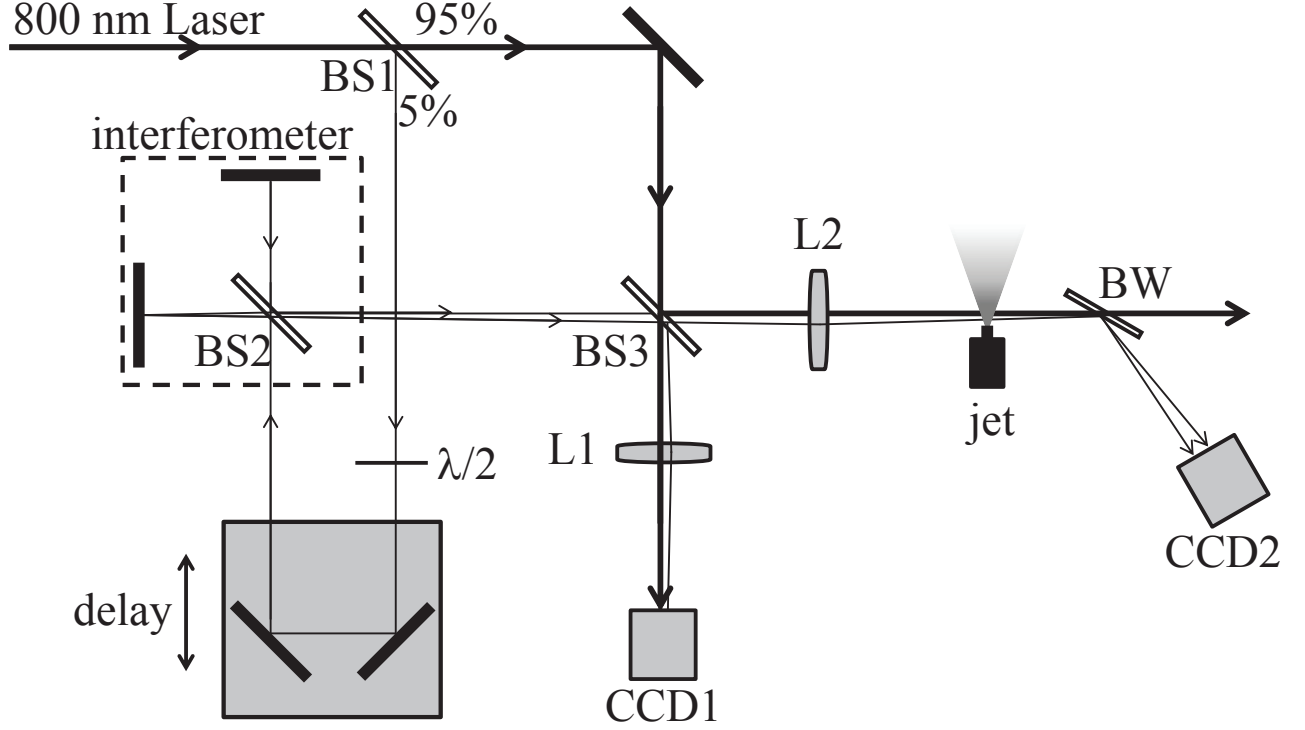


FIG. 2. A schematic diagram of the laser system. The plasma is created by focusing a high power laser beam into a Ne gas jet. Two weak laser beams from a slightly misaligned Michelson interferometer probe the plasma as described in the text. BS1, BS2, BS3 = beam splitters. L1, L2 = lenses. CCD1, CCD2 = CCD cameras. BW = window at Brewster's angle.  $\lambda/2$  = half-wave plate. CCD1 is used to verify the focal spot alignment as the delay line moves. CCD2 is used to measure the interference fringes in the two weak laser beams.

limiting the peak laser intensity in the gas jet to  $2.5 \times 10^{15} \text{ W/cm}^2$ .

The plasma density is measured by determining the phase shift of a probe laser beam as it passes through the plasma. A schematic diagram of the laser system is shown in Fig. 2. The main laser beam is divided into two beams using a 95:5 beamsplitter. The more powerful beam is focused into the gas jet using a 50 cm focal length lens. The weaker beam traverses a variable-length delay line and is split again into two beams in a Michelson interferometer. The two arms of the interferometer are set to zero path-length difference. One of the mirrors is tilted by  $0.1^\circ$ , causing two laser beams to emerge, called the probe and reference beams. They are combined with the strong beam at the focusing lens. All three laser beams are focused by the same lens into the Ne gas jet. The weak probe is aligned to pass through the center of the plasma created by the strong beam. The weak reference beam focuses about 1 mm to the side of the plasma. All three laser beams exit the vacuum chamber through a window. A glass plate at Brewster's angle reflects the probe and reference laser beams while passing the strong beam into a beam dump. The probe and reference laser beams overlap in the far field and form an interference pattern on CCD2 (see Fig. 2), analogous to a Young's double-slit interference pattern. The fringes in the interference pattern shift depending on the phase shift accrued by the probe laser beam as it passes through the plasma. Typical fringe data is shown in Fig. 3.

The index of refraction,  $\tilde{n}$ , of a plasma of free electrons is given by  $\tilde{n} = [1 - (\omega_p/\omega_L)^2]^{1/2}$ , where  $\omega_p = \sqrt{ne^2/m_e\epsilon_0}$  is the electron plasma frequency and  $\omega_L$  is the laser frequency. As the index of refraction changes, the fringes in the interference pattern shift because of changes in the relative phase of the probe and reference laser beams,

$$\Delta\phi = \frac{2\pi L}{\lambda}(1 - n) \approx nL \frac{e^2}{2m\epsilon_0\omega_L c}. \quad (4)$$

The fringe shift, measured in pixel number on CCD2, is converted to phase by equating the period of the interference pattern to a phase shift of  $2\pi$ . Then Eq. (4) is used to determine the density of the plasma. By changing the delay of the two weak beams relative to the strong laser beam, we measure the plasma density as a function of time. Typical results are shown in Fig. 4.

The left panel of Fig. 4 shows the measured fringe shift in pixels as a function of the distance of the delay arm for

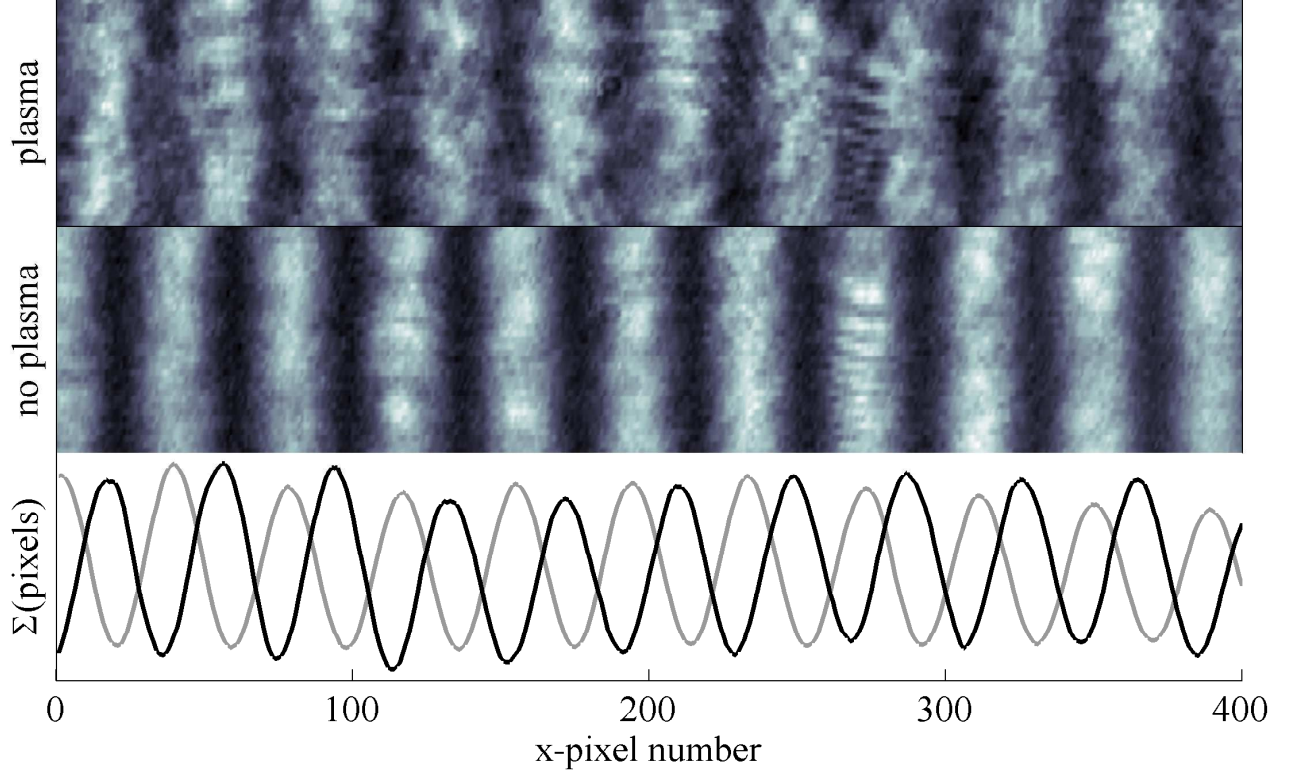


FIG. 3. Interference fringes as measured using camera CCD2. Top panel: fringes when the plasma is present. Middle panel: fringes when the plasma is absent. Bottom panel: the vertical sum of the fringe shift image data with the background subtracted. The time delay is 100 ps and the plasma density is  $n = 1.3 \times 10^{18} \text{ cm}^{-3}$ . Each image is an average of 10 laser pulses.

three different plasma conditions. From this data we can extract the electron temperature, as shown in the right-hand panel of Fig. 4. The relative plasma density is plotted as a function of time. All three densities show the same overall behavior. Using the expression for a symmetric two-dimension symmetric expansion,

$$n(t) = \frac{n(0)}{1 + (v_{\text{exp}}t/\sigma_0)^2} \quad (5)$$

we fit our data to extract  $\sigma_0/v_{\text{exp}} = 4.8 \text{ ns}$ . We measure the Gaussian width of the ionizing laser beam focus to be  $w = 70 \text{ }\mu\text{m}$ . The peak intensity in the laser pulse is calculated to be  $2.5 \times 10^{15} \text{ W/cm}^2$ . The radius at which the laser beam falls below the critical intensity of  $8.7 \times 10^{14} \text{ W/cm}^2$  required to ionize neon is  $0.73w$ . A flat distribution of radius  $0.73w$  has an rms size of  $\sigma = 0.42w = 29 \text{ }\mu\text{m}$ . Therefore the plasma expansion velocity is 6000 m/s, giving an electron energy of  $k_B T_e = m_i v_{\text{exp}}^2 = 15 \text{ eV}$ .

We can estimate the expected electron energy using a model based on strong-field ionization. After the electron is detached, the Coulomb field from the parent ion is negligible compared to the laser field. An electron with charge  $e$  accelerates in the laser field  $\mathcal{E} = E_0 \cos(\omega t + \phi)$ . For an electron initially at rest, the velocity of the electron at some later time  $t$  will be

$$\dot{x} = \frac{eE_0}{\omega m} [\sin(\omega t + \phi) - \sin \phi] \quad (6)$$

The average drift kinetic energy of the electron after the laser pulse is finished will be the time-averaged quantity  $\langle K_{\text{drift}} \rangle = 2U_p \langle \sin^2 \phi \rangle_\phi$ , where  $U_p = e^2 E_0^2 / 4\omega^2 m$  is the ponderomotive energy. The average occurs over phase angles  $\phi$  in which the electron can escape from the atom. For example there can be some detachment phases such that the quivering electron drifts towards the parent ion and other times such that it drifts away. A reasonable choice of phase range is  $\phi = \pm\pi/6$ , giving

$$\langle K_{\text{drift}} \rangle = 0.17U_p. \quad (7)$$

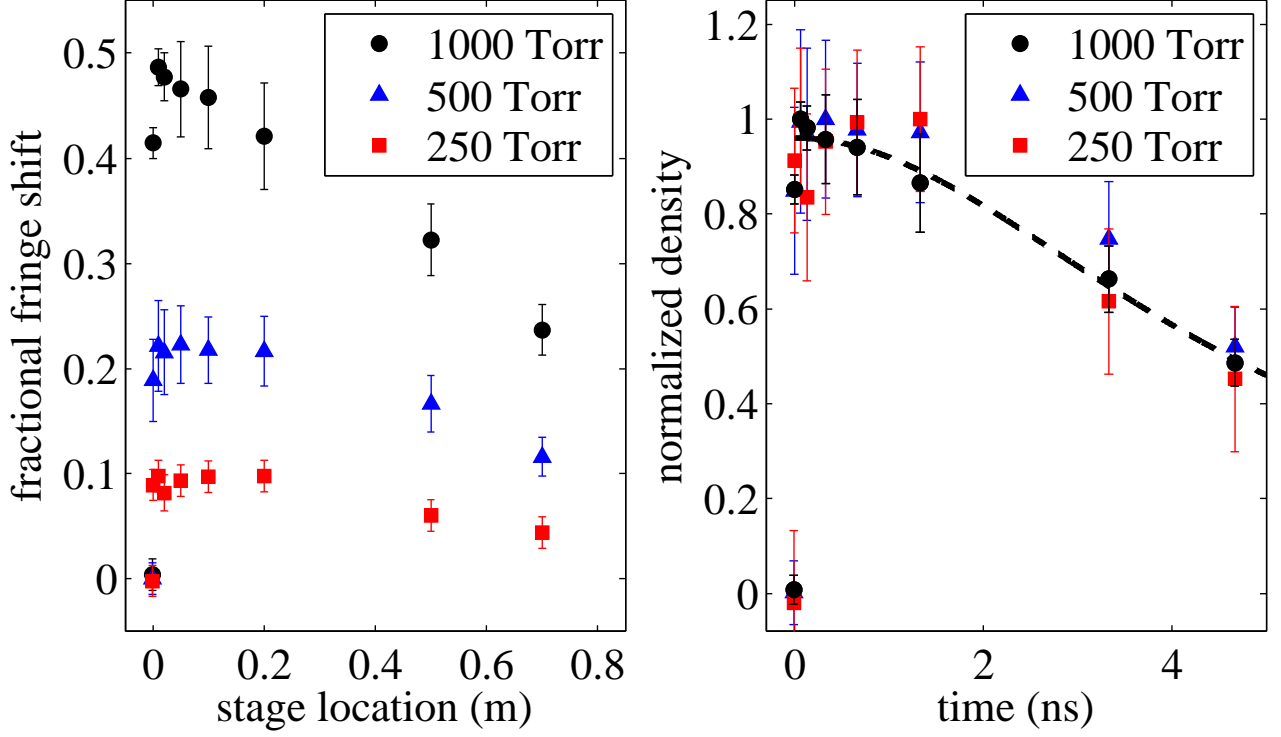


FIG. 4. Fringe shift and plasma density as a function of time after plasma creation for three different pressures behind the jet. The maximum fringe shift corresponds to a plasma density of  $1.3 \times 10^{18} \text{ cm}^{-3}$  and is directly proportional to the pressure behind the jet. The right panel shows the scaled density as a function of time. The data from all three initial densities follows the same curve, indicating that there is no significant recombination at these time scales. The UNP expansion model of Eq. (5) is plotted as the dashed line for  $k_B T_e = 15 \text{ eV}$ .

In our experiment, with a peak intensity of  $2.5 \times 10^{15} \text{ W/cm}^2$ , the ponderomotive energy is 150 eV, suggesting an electron energy of 25 eV, in rough agreement with our measurement (15 eV).

A strong connection between our LPP and UNPs can be drawn in consideration of the ion temperature. Initially the neutral atom temperature in our effusive jet is near room temperature, about 300 K. When the plasma is formed, the inter-particle potential energy landscape impulsively hardens[24]. The 35 fs laser pulse is short compared to the ion plasma frequency,  $\omega_p^i = (2.8 \text{ ps})^{-1}$  at a density of  $1.5 \times 10^{18} \text{ cm}^{-3}$ . The ions will move to minimize their potential energy due to interactions with neighboring ions. On the time scale of the ion plasma frequency, they will reach the correlation temperature  $T_c = (2/3)(e^2/4\pi\epsilon_0 a_{ws} k_B) = 3000 \text{ K}$  where  $a_{ws} = (3/4\pi n)^{1/3}$  is the Wigner-Seitz radius. Although the neutral atoms are initially at room temperature, their equilibrium temperature is much higher and determined by the plasma density. This same phenomenon, called disorder-induced heating [8, 24–27], has been studied extensively in ultracold neutral plasmas. Because the density determines the ion temperature, UNP physics can be studied in LPPs at room temperature.

Research with UNPs suggests that three-body recombination becomes important when the electron Coulomb coupling parameter is  $\Gamma = Z^2 e^2 / 4\pi\epsilon_0 a_{ws} k_B T_e > 0.1$  [15, 28], where  $Z$  is the ionization state. For a plasma with an electron temperature of 15 eV, this happens at a density of  $3 \times 10^{20} \text{ cm}^{-3}$ , or about 10 times ambient density. However, the three-body recombination rate depends on temperature as  $T_e^{-9/2}$ , meaning that lower temperatures lead to significantly greater recombination. Xenon, for example, can be ionized at 10 times lower laser intensity than what is required for neon. The model of Eq. (7) suggests that in a xenon LPP with our density of  $n = 1.5 \times 10^{18} \text{ cm}^{-3}$  and ten times lower laser intensity the recombination rate ( $\approx (50 \text{ ps})^{-1}$ ) would have a noticeable effect on the density evolution on the sub-ns time scale.

In conclusion, we have shown that UNPs and a certain class of cool low-density LPPs are similar. They are both quasi-neutral plasmas in which the plasma expansion is driven by the electron pressure. They both are treated successfully using an analytic solution of the plasma equations that assumes local thermodynamic equilibrium. The analytic solutions originally developed for UNPs can be used to predict the LPP electron temperature. At the densities achieved in our experiment, the ions are strongly coupled because the ion temperature at early times is determined by

the density. Calculations suggest that under some readily attainable experimental conditions the electrons can also be strongly coupled.

Future studies could explore the influence of the laser intensity on the electron temperature as suggested by Eq. (7). Plasmas with strong coupling in both the electrons and ions are of great fundamental interest. It should be possible to generate plasmas with even higher values of  $\Gamma$  using LPPs generated by a sequence of laser pulses, as suggested by Murillo [29]. Because  $\Gamma$  is proportional to  $Z^2$ , a carefully designed laser pulse sequence for  $Z = 5$ , for example, could potentially increase  $\Gamma$  to values greater than 20 in a neutral non-degenerate system.

### ACKNOWLEDGEMENTS

This work has been supported by NSF Grants PHY-0969856 and PHY-0970065. We gratefully acknowledge the help of Josh L. Olson in building the early stages of this experiment.

---

\* [scott.bergeson@byu.edu](mailto:scott.bergeson@byu.edu)

- [1] C. G. Morgan, *Plasma Phys. Control. Fusion* **26**, 1367 (1984).
- [2] M. J. Edwards, J. D. Lindl, B. K. Spears, S. V. Weber, L. J. Atherton, D. L. Bleuel, D. K. Bradley, D. A. Callahan, C. J. Cerjan, D. Clark, G. W. Collins, J. E. Fair, R. J. Fortner, S. H. Glenzer, S. W. Haan, B. A. Hammel, A. V. Hamza, S. P. Hatchett, N. Izumi, B. Jacoby, O. S. Jones, J. A. Koch, B. J. Koziolowski, O. L. Landen, R. Lerche, B. J. MacGowan, A. J. MacKinnon, E. R. Mapoles, M. M. Marinak, M. Moran, E. I. Moses, D. H. Munro, D. H. Schneider, S. M. Sepke, D. A. Shaughnessy, P. T. Springer, R. Tommasini, L. Bernstein, W. Stoeckl, R. Betti, T. R. Boehly, T. C. Sangster, V. Y. Glebov, P. W. McKenty, S. P. Regan, D. H. Edgell, J. P. Knauer, C. Stoeckl, D. R. Harding, S. Batha, G. Grim, H. W. Herrmann, G. Kyrala, M. Wilke, D. C. Wilson, J. Frenje, R. Petrasso, K. Moreno, H. Huang, K. C. Chen, E. Giraldez, J. D. Kilkenny, M. Mauldin, N. Hein, M. Hoppe, A. Nikroo, and R. J. Leeper, *Physics of Plasmas* **18**, 051003 (2011).
- [3] S. Banerjee, N. Powers, V. Ramanathan, B. Shadwick, and D. Umstadter, Proceedings of Particle Accelerator Conference 2009 **A14 Advance Concepts**, 1 (2009).
- [4] T. C. Killian, S. Kulin, S. D. Bergeson, L. A. Orozco, C. Orzel, and S. L. Rolston, *Phys. Rev. Lett.* **83**, 4776 (1999).
- [5] T. C. Killian, *Science* **316**, 705 (2007).
- [6] S. L. Rolston, *Physics* **1**, 2 (2008).
- [7] T. Killian, T. Pattard, T. Pohl, and J. Rost, *Physics Reports* **449**, 77 (2007).
- [8] S. D. Bergeson, A. Denning, M. Lyon, and F. Robicheaux, *Phys. Rev. A* **83**, 023409 (2011).
- [9] J. P. Morrison, C. J. Rennick, J. S. Keller, and E. R. Grant, *Phys. Rev. Lett.* **101**, 205005 (2008).
- [10] C. Deutsch, H. B. Nersisyan, and G. Zwicknagel, *AIP Conference Proceedings* **1421**, 3 (2012).
- [11] T. Kluge, T. Cowan, A. Debus, U. Schramm, K. Zeil, and M. Bussmann, *Phys. Rev. Lett.* **107**, 205003 (2011).
- [12] S. Augst, D. Strickland, D. D. Meyerhofer, S. L. Chin, and J. H. Eberly, *Phys. Rev. Lett.* **63**, 2212 (1989).
- [13] P. Mora, *Phys. Rev. Lett.* **90**, 185002 (2003).
- [14] S. Laha, P. Gupta, C. E. Simien, H. Gao, J. Castro, T. Pohl, and T. C. Killian, *Physical Review Letters* **99**, 155001 (2007).
- [15] F. Robicheaux and J. D. Hanson, *Phys. Rev. Lett.* **88**, 055002 (2002).
- [16] S. Mazevet, L. A. Collins, and J. D. Kress, *Phys. Rev. Lett.* **88**, 055001 (2002).
- [17] T. Pohl, T. Pattard, and J. M. Rost, *Phys. Rev. A* **70**, 033416 (2004).
- [18] E. P. Kanter, R. Santra, C. Höhr, E. R. Peterson, J. Rudati, D. A. Arms, E. M. Dufresne, R. W. Dunford, D. L. Ederer, B. Krässig, E. C. Landahl, S. H. Southworth, and L. Young, *Journal of Applied Physics* **104**, 073307 (2008).
- [19] P. Gupta, S. Laha, C. E. Simien, H. Gao, J. Castro, T. C. Killian, and T. Pohl, *Phys. Rev. Lett.* **99**, 075005 (2007).
- [20] *NRL Plasma Formulary* (Naval Research Laboratory, Washington, DC, 2002) p. 54.
- [21] E. A. Cummings, J. E. Daily, D. S. Durfee, and S. D. Bergeson, *Phys. Rev. Lett.* **95**, 235001 (2005).
- [22] E. A. Cummings, J. E. Daily, D. S. Durfee, and S. D. Bergeson, *Physics of Plasmas* **12**, 123501 (2005).
- [23] The value for  $\sigma_x = 16 \mu\text{m}$  is given in Fig. 4 of Ref. [18].
- [24] M. S. Murillo, *Phys. Rev. Lett.* **96**, 165001 (2006).
- [25] C. E. Simien, Y. C. Chen, P. Gupta, S. Laha, Y. N. Martinez, P. G. Mickelson, S. B. Nagel, and T. C. Killian, *Phys. Rev. Lett.* **92**, 143001 (2004).
- [26] Y. C. Chen, C. E. Simien, S. Laha, P. Gupta, Y. N. Martinez, P. G. Mickelson, S. B. Nagel, and T. C. Killian, *Phys. Rev. Lett.* **93**, 265003 (2004).
- [27] M. Lyon and S. D. Bergeson, *Journal of Physics B:Atomic, Molecular and Optical Physics* **44**, 184014 (2011).
- [28] J. L. Roberts, C. D. Fertig, M. J. Lim, and S. L. Rolston, *Phys. Rev. Lett.* **92**, 253003 (2004).
- [29] M. S. Murillo, *Physics of Plasmas* **14**, 055702 (2007).